JAMES | Journal of Advances in Modeling Earth Systems

RESEARCH ARTICLE
10.1029/2018MS001565

Key Points:
- We explore the environmental drivers to trigger off new leaf formation and old leaf shedding in Amazonian evergreen forests
- This model links leaf phenology with the seasonality of carbon allocation to leaves, roots, and sapwood
- The new phenology model leads to good representation of the seasonality of canopy photosynthesis, litterfall and latent heat

Supporting Information:
- Supporting Information S1

Correspondence to:
X. Chen,
chenxzh73@mail.sysu.edu.cn;
chenxiuzhicas@gmail.com

Citation:
Chen, X., Maignan, F., Viovy, N., Bastos, A., Goll, D., Wu, J., et al. (2020). Novel representation of leaf phenology improves simulation of Amazonian evergreen forest photosynthesis in a land surface model. *Journal of Advances in Modeling Earth Systems*, *12*, e2018MS001565. https://doi.org/10.1029/2018MS001565

Received 8 DEC 2018
Accepted 29 NOV 2019
Accepted article online 6 DEC 2019

Novel Representation of Leaf Phenology Improves Simulation of Amazonian Evergreen Forest Photosynthesis in a Land Surface Model

Xiuzhi Chen[1,2,3], Fabienne Maignan[2], Nicolas Viovy[2], Ana Bastos[2,4], Daniel Goll[2], Jin Wu[5,6], Liyang Liu[2,3], Chao Yue[7], Shushi Peng[8], Wenping Yuan[1,3], Adriana Castro da Conceição[9], Michael O'Sullivan[10], and Philippe Ciais[2]

[1]School of Atmospheric Sciences, Center for Monsoon and Environment Research, Sun Yat-Sen University, Guangzhou, China, [2]Laboratoire des Sciences du Climat et de l'Environnement/IPSL, UMR 8212 CEA-CNRS UVSQ, Gif-sur-Yvette, France, [3]Southern Marine Science and Engineering Guangdong Laboratory (Zhuhai), Zhuhai, China, [4]Department of Geography, Ludwig-Maximilians University, Munich, Germany, [5]Department of Environmental and Climate Sciences, Brookhaven National Laboratory, Upton, NY, USA, [6]School of Biological Sciences, The University of Hong Kong, Pokfulam, Hong Kong, [7]State Key Laboratory of Soil Erosion and Dryland Farming on the Loess Plateau, Northwest A&F University, Yangling, China, [8]Sino-French Institute for Earth System Science, College of Urban and Environmental Sciences, Peking University, Beijing, China, [9]National Institute for Amazonian Research (INPA), C.P. 478, Manaus, Brazil, [10]College of Life and Environmental Sciences, University of Exeter, Exeter, UK

Abstract Leaf phenology in the humid tropics largely regulates the seasonality of forest carbon and water exchange. However, it is inadequately represented in most global land surface models due to limited understanding of its controls. Based on intensive field studies at four Amazonian evergreen forests, we propose a novel, quantitative representation of tropical forest leaf phenology, which links multiple environmental variables with the seasonality of new leaf production and old leaf litterfall. The new phenology simulates higher rates of leaf turnover (new leaves replacing old leaves) in dry seasons with more sunlight, which is then implemented in ORCHIDEE, together with recent findings of ontogeny-associated photosynthetic capacity, and is evaluated against ground-based measurements of leaf phenology (canopy leaf area index and litterfall), eddy covariance fluxes (photosynthesis and latent heat), and carbon allocations from field observations. Results show the periodical cycles of solar radiation and vapor pressure deficit are the two most important environmental variables that are empirically related to new leaf production and old leaf abscission in tropical evergreen forests. The model with new representation of leaf phenology captures the seasonality of canopy photosynthesis at three out of four sites, as well as the seasonality of litterfall, latent heat, and light use efficiency of photosynthesis at all tested sites, and improves the seasonality of carbon allocations to leaves, roots, and sapwoods. This study advances understanding of the environmental controls on tropical leaf phenology and offers an improved modeling tool for gridded simulations of interannual CO_2 and water fluxes in the tropics.

1. Introduction

The tropical evergreen forest of Amazonia holds 34% of terrestrial carbon stocks and makes up a significant fraction of the global carbon sink (Beer et al., 2010; Pan et al., 2011; Rödig et al., 2018). Improved model representation of the region's carbon and water fluxes is important if we are to assess their ongoing and future changes (Fu et al., 2013; Peñuelas & Filella, 2009; Wright et al., 2017). However, most Earth system models (ESMs) still fail to accurately model the responses of Amazonian evergreen forest to seasonal and interannual climatic variations; this is in part due to the poor representation of tropical phenology in current ESMs (Restrepo-Coupe et al., 2017; Wu et al., 2016).

Despite its perennial canopy, the Amazonian evergreen forest shows significant leaf phenology, that is, seasonal variation in satellite-detected greenness (Bi et al., 2015; Huntingford et al., 2013; Saleska et al., 2016; Schimel et al., 2015; Wu et al., 2018) and ground-detected variation in leaf age cohorts, with cohorts of new leaves emerging and increasing in the dry season (Doughty & Goulden, 2008; Brando et al., 2010; Lopes et al., 2016; Wu et al., 2016; Detto et al., 2018). Although the seasonality is modest, compared to other regions, several recent studies converge to show that tropical leaf phenology dominates regulating the

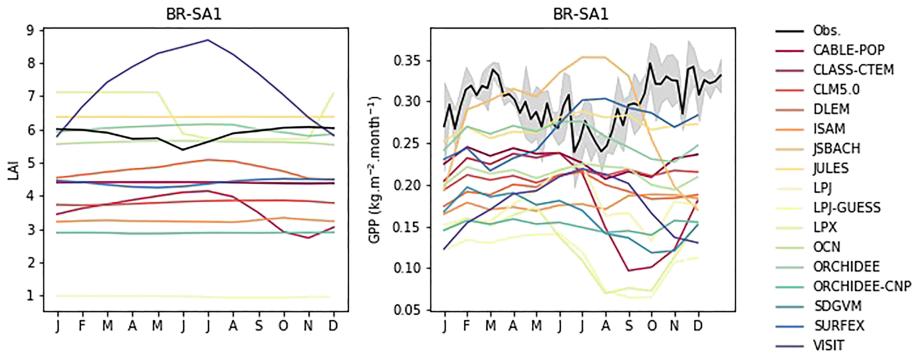

Figure 1. Mean seasonality of simulated *LAI* and *GPP* at the BR-Sa1 site from Trendy V7, plus observations. (a) *LAI*; (b) *GPP*.

seasonal cycles of carbon and water fluxes (Albert et al., 2018; Doughty & Goulden, 2008; Wu et al., 2016). The underlying reason is the higher leaf turnover (newly produced leaves replacing old leaves) during the dry season (Brando et al., 2010; Lopes et al., 2016; Wu et al., 2016; Detto et al., 2018), with new maturing leaves having higher leaf-level photosynthetic capacity (PC) than the old leaves being replaced. This phenomenon drives a dry season increase in canopy photosynthesis.

Despite the importance of leaf phenology in the forests of the humid tropics, it remains unclear what climatic and biotic drivers provide the predominant control on leaf drop and leaf flush timing (Tang & Dubayah, 2017). Several hypotheses from former studies (Saleska et al., 2003) suggested that leaf onset may be driven by precipitation, soil moisture, or vapor pressure deficit (*VPD*), which are related to water availability (Asner & Alencar, 2010; Brando et al., 2010; Davidson et al., 2012; Lee et al., 2013; Saleska et al., 2016). Leaf onset may also be related to higher shortwave downwelling radiation (*SWdown*) or photosynthetically active radiation (*PAR*), that is, to more sunlight being available at the top of canopy (Bi et al., 2015; Guan et al., 2015; Xu et al., 2011; Huete et al., 2006; Wu et al., 2016). Thus, the environmental triggers driving the leaf phenology are uncertain (Bi et al., 2015; Huete et al., 2006; Morton et al., 2014; Wu et al., 2018).

Only few land surface models (LSMs) attempted to represent the seasonality of canopy photosynthesis in evergreen tropical forests: the Simple Biosphere model (Baker et al., 2008), Lund-Potsdam-Jena managed Land model (Saleska et al., 2003), Terrestrial Ecosystem Model (Poulter et al., 2009), Organizing Carbon and Hydrology in Dynamic Ecosystems model (ORCHIDEE) (de Weirdt et al., 2012), and the ecohydrological model Tethys and Chloris. However, most of these models fail to relate the leaf flushing (de Weirdt et al., 2012) or the leaf shedding (Manoli et al., 2018) or both to climatic drivers. Figure 1a lists the mean seasonality of simulated leaf area index (*LAI*) at the BR-Sa1 site across 16 LSMs from the Trendy V7 exercise (Sitch et al., 2013; Peng et al., 2015; Le Quéré et al., 2018). We see that most simulated *LAI* either show little seasonal variability throughout the year or exhibit a significant drop in the dry season that contrasts with the camera-based observations (Figure 3 in Wu et al., 2016). Regarding the performances of these LSMs in simulating tropical gross primary production (*GPP*) seasonality, up to 13 out of 16 LSMs show a remarkable *GPP* decrease during the dry season period (Figure 1b), which is not in agreement with the eddy covariance flux at BR-Sa1 site. Obviously, there is a large spread across current LSMs and satellites regarding the seasonality of *LAI* and *GPP* products.

In addition, although seasonal variation in carbon allocation to leaves, stems, and roots are now measured regularly at field sites, these processes remain poorly represented in most ESMs. For example, when Amazonian evergreen forests enter the early dry season, allocation of carbohydrates to new leaves was found to increase, while the allocation to stems and roots decreased, in the data presented by Poorter et al. (2012), Doughty et al. (2015), and Restrepo-Coupe et al. (2016). By contrast, many models have constant carbon allocation coefficients for leaves, stems, and roots for tropical evergreen forests (Krinner et al., 2005; Potter et al., 2001). Obviously, the mismatch between modeled and observed carbon seasonal allocation to leaves versus stems and roots is related to the poor representation of leaf seasonality. Therefore, we expect an improved

Table 1
Description of the Four Eddy Covariance Flux Tower Sites in Amazonian Forest

Sites	Name	Longitude (°)	Latitude (°)	Soil type	Precipitation (mm/year)		*SWdown* (W/m^2)		*PAR* ($\mu mol \cdot m^{-2} \cdot s^{-1}$)	
					Dry	Wet	Dry	Wet	Dry	Wet
BR-Sa1	Santarem-Km67	−55	−2.85	Ferralsols (FAO) /Oxisols (USDA)	917	1,610	236	193	381	326
BR-Sa3	Santarem-Km83	−55	−3.02	Ferralsols (FAO) /Oxisols (USDA)	308	1,102	205	172	357	281
BR-Ma2	Manaus-Km34	−60.2	−2.61	Ferralsols (FAO) /Oxisols (USDA)	653	1,481	213	192	421	341
GF-Guy	Guyaflux (French Guiana)	−52.9	5.28	Acrisols (FAO)	756	2,366	225	174	500	400

understanding of tropical forest leaf phenology should also lead to improved simulation of carbon allocation to stems and roots.

This study focuses on the process of coincident production of new leaves and litterfall of old leaves, which implies that more carbon gets allocated to new leaves and that the shedding rate of old leaves is increased just before to produce a younger leaf age demography in the canopy; this process is important in producing the higher photosynthetic rates of the dry season (Chave et al., 2010; de Weirdt et al., 2012; Wagner et al., 2012; Wu et al., 2017; Xu et al., 2017). This argument is supported by field observations from Wu et al. (2016) and by Xu et al. (2017) of ontogeny-associated PC. In this paper, we (1) illustrate the fact that current LSMs do not capture the seasonality of tropical evergreen forests phenology; (2) explore environmental drivers that trigger new leaf formation and old leaf shedding in Amazonian evergreen forests; (3) link leaf phenology with the seasonality of carbon allocation to leaves, roots, and sapwood in the equations of the ORCHIDEE LSM, with a parsimonious modeling strategy; and (4) simulate the seasonality of canopy leaf phenology, carbon and water fluxes, and litterfall and evaluate model results with observations.

In the canopy photosynthesis submodel of the ORCHIDEE LSM, the shifts in carbon allocation to new leaves and the litterfall of old leaves are defined by empirical functions of *SWdown* and *VPD*, respectively, combined with an ontogeny-dependent leaf PC function (Xu et al., 2017). Model results are tested in two steps. First, we fix the dates on which new leaves are triggered. This procedure tests only the new carbon allocation and leaf demography model: The fixed dates are adjusted to best reproduce the observed seasonal cycles of *GPP* measured at four sites. Second, we model the onset of young leaves from *SWdown* and *VPD* drivers. The model outputs are evaluated against in situ camera observations of *LAI* cohorts, litterfall, carbon allocation, and eddy covariance measurements of *GPP* and evaporation (*LE*) at four forest sites in Amazonia.

2. Sites and Data

2.1. Sites

Four eddy covariance flux tower sites (BR-Sa1, BR-Sa3, BR-Ma2, and GF-Guy, see Table 1) located in Amazonian evergreen forest were selected for model evaluation (Keller et al., 2001; Araújo et al., 2002; Wu et al., 2016; Bonal et al., 2008). All the meteorological variables show significant seasonality at each of the four sites. The average rainfall rates in the wet season at BR-Sa1, BR-Sa3, BR-Ma2, and GF-Guy are, respectively, 1.8, 3.6, 2.3, and 3.1 times higher than those in the corresponding dry season. Similarly, the *SWdown* during the dry season is 22%, 19%, 11%, and 29% higher than during the wet season, and *PAR* in the dry season is on average 16%, 17%, 23%, and 25%, respectively, higher than during the wet season. In summary, the meteorological seasonal variability at the four sites shows enhanced light availability and reduced water availability during the dry season as compared to the wet season. The periods of the precipitation, *SWdown*, and *PAR* data are listed in supporting information Table S1. The timing of the dry and wet seasons at the four sites are defined using *VPD*, as listed in Table 2. The dry seasons at the four sites always happen during the second half of the year.

Table 2
Empirically Based Dates (Unit: Weeks Since the First Week of the Calendar Year) When Mean Anomalies of Environmental Factors (Precipitation, SWdown and VPD) Change Sign and of Beginning of the Mean Canopy Rejuvenation Period Determined by LAI_{young} at Four Eddy Covariance Flux Tower Sites in Amazonia

	Date (unit: weeks) according to environmental factors, that is			
Sites	Precipitation	*SWdown*	*VPD*	LAI_{young}
BR-Sa1	24	26	27	28
BR-Sa3	25	25	26	28
BR-Ma2	24	26	27	28
GF-Guy	27	27	30	28

2.2. Simulation Setup for the ORCHIDEE Model

For each site, ORCHIDEE was forced using 30-min average top-of-tower observations of *SWdown*, longwave downwelling radiation (*LWdown*), air temperature, air humidity, precipitation, wind speed, and surface pressure. The vegetation at the four sites was set to the plant functional type evergreen broadleaf forest, with 100% cover. The soil types, used to define soil textures in the soil hydrology model, are shown in Table 1 (de Weirdt et al., 2012; Malhi et al., 2009). The ORCHIDEE parameter of maximum *LAI* (m^2/m^2) was set to 6 according to de Weirdt et al. (2012) and Wu et al. (2016). When *LAI* reaches this maximum value, no more carbon is allocated to leaves (as described in Section A5 of Krinner et al., 2005). Xu et al. (2017) observed that canopy leaf mass per area (LMA) differ significantly among Amazonian evergreen forest sites (Figure S1), but understory LMA (Figure S1) and maximum carboxylation rate ($V_{c,max}$) (Figure S2) only differ slightly. So, a constant maximum $V_{c,max}$ value (51.4 $\mu mol \cdot m^{-2} \cdot s^{-1}$) was prescribed at all the four sites, and we also ignore the differences of understory LMA. For canopy differences, the specific leaf area (SLA = 1.0/LMA) was fixed to a value of 15.3 mm^2/mg C. This corresponds to a LMA value of 65 g/m^2, within the range of 10–250 observed by Xu et al. (2017) across species and sites. This SLA value is set for the oldest leaf age class, and we applied scaling factors, of 0.8, 0.85, and 0.9, to decrease the SLA for leaf Age Classes 1 to 3, respectively, as younger leaves are thinner.

A first spin-up was run for all sites by recycling climate forcing data during the period 1980–2010 for more than 300 years until all vegetation carbon pools had reached a steady state (Traore et al., 2014) using the model spin-up approach described by Lardy et al. (2011). After that, we carried out a set of simulations from the end of the spin-up state during the periods of observation coverage at each site (Table S1).

2.3. Observed *LAI*, Carbon Allocation Fractions, Litterfall, *GPP*, and *LE*

Mean monthly *LAI* cohorts were calculated from top-of-canopy images of a Tetracam Agricultural Digital Camera at the BR-Sa1 site from January 2000 to December 2005 (Wu et al., 2016). The camera-inferred *LAI*s were classified into three cohorts based on different leaf ages: young (<2 months); mature (3–5 months); old (>6 months). Detailed information on camera data processing is given by Wu et al. (2016).

Aboveground total litterfall at BR-Sa1 site was collected approximately every 14 days using 40 circular, mesh screen traps randomly located throughout the 19.75-ha tree survey areas (Rice et al., 2004). Litterfall at BR-Sa3 was measured in an 18-ha plot adjacent to the eddy flux tower using 30 litter baskets and collected every 14 days (Figuera et al., 2011). Litterfall at the BR-Ma2 site was collected from 0.5 m^2 traps at monthly interval on 25 traps randomly located in a 1-ha plot (Wu et al., 2016). Litterfall at the GF-Guy site was collected approximately every 20 days in 40 different traps distributed at the corners of 10 inventory plots located in the eddy covariance footprint of the GF-Guy tower (de Weirdt et al., 2012).

The monthly mean fractions of carbon allocated to leaves (f_{leaf}), roots (f_{root}), and sapwood (f_{sap}) were taken from the observations at the Tambopata and Caxiuanã sites by Doughty et al. (2015). The Caxiuanã site is very close to (~410 km) the BR-Sa1 site (Figure S3), and its climate, forest, and soil type (Table S2) are also comparable to those of the BR-Sa1 site. As there are very few Amazonian forest sites where allocation data are available, we used here the field allocation data of the BR-Sa1 site to evaluate the simulated carbon allocation fractions at the BR-Sa1 site.

To evaluate the simulated results, we used the daily averaged *GPP* ($g\ C \cdot m^{-2} \cdot day^{-1}$), latent heat fluxes (*LE*) ($W\ m^{-2}$) from the eddy covariance flux tower sites, survey-collected total litterfall ($g\ C \cdot m^{-2} \cdot day^{-1}$), mean monthly camera-observed *LAI* cohorts, and fractions of carbon allocated to roots, leaves, and sapwood.

We selected data from the FLUXNET 2015 database (https://fluxnet.fluxdata.org/data). Eddy covariance measured *GPP* in the database was calculated half-hourly following the methods described on the website http://fluxnet.fluxdata.org/data/fluxnet2015-dataset/data-processing/ (Papale et al., 2006). The net ecosystem exchange (*NEE*, $g\ C \cdot m^{-2} \cdot day^{-1}$) of CO_2 was partitioned into ecosystem respiration (*Resp*, $g\ C \cdot m^{-2} \cdot day^{-1}$) and *GPP* using the method of Restrepo-Coupe et al. (2013). *Resp* was averaged into monthly bins from valid nighttime hourly *NEE* during well-mixed periods (friction velocity ≥ 0.22 m/s; Hutyra et al., 2007; Wu et al., 2016), and *GPP* was estimated as $GPP = NEE - Resp$.

The time periods of eddy covariance flux tower data and litterfall are presented in Table S1.

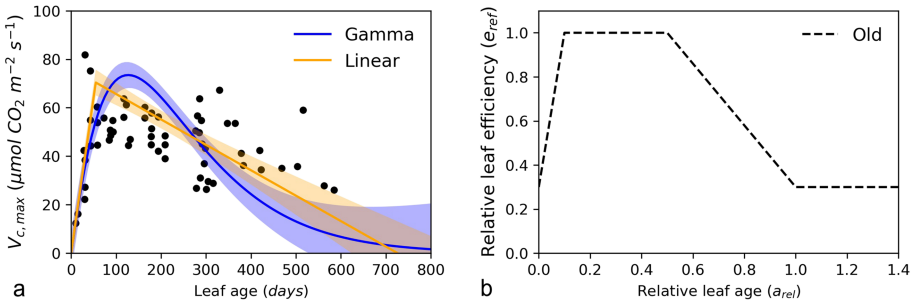

Figure 2. (a) $V_{c,max}$ and (b) relative leaf efficiency (e_{rel}) as a function of relative leaf age (a_{rel}). "Old" indicates the leaf efficiency formula in the former version of ORCHIDEE; "Linear" is a linear fitting of $V_{c,max}$ implemented in the updated scheme (orange) and "Gamma" a gamma function fitting, both used in the new version. Colored bands indicate the 95% confidence intervals.

3. Methods

3.1. The ORCHIDEE Model

ORCHIDEE simulates exchanges of water, momentum and greenhouse gases between the atmosphere and the terrestrial biosphere (Krinner et al., 2005). The modeled carbon processes include phenology, photosynthesis, respiration, allocation, and leaf shedding (Figure 2 in Krinner et al., 2005). The standard ORCHIDEE version (v8.4.1) used here was recently evaluated over high latitudes (Guimberteau et al., 2017; Guimberteau et al., 2018). Because the model is known to perform poorly for tropical phenology (De Weirdt et al., 2012; Sitch et al., 2013; Peng et al., 2015); we investigated the canopy phenology of tropical evergreen forests aiming to improve the modeling of the processes of leaf growth and leaf shedding in the ORCHIDEE.

The model accounts for age-related decline in leaf-scale PC through a variable maximum rate of carboxylation of leaves with leaf age. ORCHIDEE has four leaf-age classes in the canopy, the age distribution being constant throughout the canopy depth. The four leaf-age classes or cohorts are characterized by their fractions of total leaf biomass and mean age. The leaf Class 1 represents the youngest age cohort and Class 4 represents the oldest cohort. To make observations and simulations comparable, we only present results for two age categories. The modeled leaves older than 6 months were grouped together into a unique old class, like in Wu et al. (2016), and leaves younger than 6 months constitutes the young class. More precisely, modeled Cohorts 2 to 4 are merged into the old class contributing to LAI_{old}, and Cohort 1 corresponds to LAI_{young}.

Wu et al. (2016) observed a similar seasonality of LAI_{young} at both the BR-Sa1 and BR-Sa3 sites. An increasing LAI_{young} indicates the flushing of new leaves and canopy rejuvenation. Canopy rejuvenation at BR-Sa1, BR-Sa3, and BR-Ma2 occurs during the dry season (second half of the calendar year), while oppositely canopy rejuvenation at GF-Guy seems to happen during the wet-season period (first half of the year, see section 3.3.2.2).

3.2. Former Model Formulations

3.2.1. Former Age-Dependent Leaf Photosynthetic Efficiency

Leaf-scale photosynthesis is calculated using the Farquhar et al. (1980) biochemical model. The stomatal conductance is a function of carbon assimilation, atmospheric CO_2 concentration, and *VPD* following the Yin et al. (2009) model. The enzyme kinetic models of photosynthesis (Farquhar et al., 1980) simulate net carbon assimilation (equation A2 in Krinner et al., 2005) using the minimum of the RuBisCO-limited carboxylation rate (equation A4 in Krinner et al., 2005) and electron transport-limited carboxylation rate (equation A5 in Krinner et al., 2005). The $V_{c,max}$ at 25 °C is scaled by a relative leaf efficiency parameter (e_{rel}, unitless: 0–1) (Ishida & Toma, 1999, Figure 2) which is a function of relative leaf age (a_{rel}, unitless: 0–1). The value of a_{rel} is calculated as the ratio of the leaf age in a cohort to the critical leaf age (a_{crit}), or leaf longevity. Following Schoettle and Fahey (1994), a_{crit} is set to 730 days for the evergreen tropical forest plant functional type (PFT). Leaf efficiency e_{rel} at leaf flushing ($a_{rel} = 0$) is given an initial value of 0.3, then increases to reach a maximum value of 1.0 at $a_{rel} = 0.01$, stays constant until $a_{rel} = 0.5$, and finally drops

back linearly to the minimum value of 0.3 at $a_{rel} = 1.0$ for the oldest leaves (Figure 2b). The leaf age and a_{crit} are used to determine the fraction of leaves that is shed (Krinner et al., 2005).

3.2.2. Former Leaf Demography Model

The default canopy demography model of ORCHIDEE has three processes solved on a daily time step: carbohydrate allocation to new leaves in Class 1, turnover from leaf age Class i to the next older one $i + 1$, and leaf shedding.

For the carbon allocation process (new leaf development), the fractions of net primary production (*NPP*) allocated to the growth of leaves (f_{leaf}) (equation A36 in Krinner et al., 2005), roots (f_{root}), sapwood (f_{sap}), and storage and reproduction organs all depend on water and light stress (Krinner et al., 2005). *NPP* allocated to leaves is transferred into the first leaf age class. Water stress on photosynthesis (carboxylation rates) and stomatal conductance is a dimensionless scalar calculated from relative soil moisture in the root zone. These stress factors are weighted according to the exponential root density profile which decreases with depth and is fixed in the model for a particular PFT; that is, they are independent of the dynamic biomass of the fine roots (equation A18 in Krinner et al., 2005).

For the leaf turnover, a constant fraction of the leaf biomass of Class i is transferred to Class $i + 1$ (equation A26 in Krinner et al., 2005) at each daily time step, and the ages of the four leaf classes are updated accordingly (equation A27 in Krinner et al., 2005). For leaf shedding, this process starts when a leaf age class reaches an age larger than half the value of a_{crit}. Then, leaf loss rapidly increases (with a power law of exponent 4) as the age of the oldest leaf class approaches the critical leaf age (equation A22 in Krinner et al., 2005). There is no leaf onset but only leaf aging and canopy rejuvenation in the former version of ORCHIDEE model.

3.3. New Model Developments

3.3.1. Updated Model of Age-Dependent Leaf Photosynthetic Efficiency

Xu et al. (2017) established a leaf age-related $V_{c,max}$ function based on field data that were collected in 20 tropical evergreen forests. Differing from the default leaf efficiency model described above (black dotted line in Figure 2b), this function gives a $V_{c,max}$ which increases rapidly for the first 2 months and then declines continuously with leaf age, after reaching the maximum $V_{c,max}$ (Figure 2a). Accordingly, we set the maximum $e_{rel} = 1$ to be reached at $a_{rel} = 0.08$.

There are few observations of $V_{c,max}$ at the a_{crit} maximum leaf age. Although some studies suggested a minimum e_{rel} between 0.10 and 0.20 for old leaves in evergreen forests (Niinemets et al., 2015), other studies observed a lower minimum e_{rel} of about 0.05 (Misson et al., 2006). Based on the observations of Xu et al. (2017), we firstly adjusted two linear functions represented by the orange curve on Figure 2a, setting a minimum efficiency $e_{rel} = 0$, both at leaf flushing ($a_{rel} = 0$) and for the oldest leaves ($a_{rel} = a_{crit}$). We also used a gamma function to fit the data of $V_{c,max}$ versus age (blue curve in Figure 2a). In both curve fits, $V_{c,max}$ would reach values close to 0 at age older than 730 days, but this critical leaf age is never reached in ORCHIDEE model given the cohorts turnover and leaf longevity.

3.3.2. Updated Leaf Demography Model

Field data (Wu et al., 2016) shows that the fraction of old leaves sharply decreases just before or at the beginning of the dry season, and this process is coincident with an increase in the fraction of new leaves (Doughty et al., 2015; Wu et al., 2016). Compared to an older canopy, a younger canopy has larger overall photosynthetic efficiency and higher *GPP* for the same amount of leaves and environmental conditions. Therefore, canopy rejuvenation thus maximizes *GPP* when radiation is highest.

In this study, the leaf flushing and shedding mechanisms were modified by introducing environmental parameters and coefficients into the original formulations (equations A36 and A22 in Krinner et al., 2005). This change simultaneously increases the rate of carbon allocation to new leaves and accelerates the shedding rate of old leaves during the canopy rejuvenation period.

3.3.2.1. New Leaf Flushing Scheme

Light availability is a major constraint on the allocation of carbon to leaves in Amazonian evergreen forest (Tang & Dubayah, 2017). Here, we assume that f_{leaf} is related to the light transmission of old leaves, being an exponential decreasing function of the leaf area index (*LAI*) of the oldest class ($-0.5^* LAI_4$) (He et al., 2017).

The fraction of *NPP* allocated to new leaves in ORCHIDEE is given in equation (1), driven by *SWdown* and the vegetation optical depth of old leaves.

$$f_{leaf}^{new} = \min\left[0.99, \left(S \times e^{-0.5LAI_4}/C_1\right)^{C_2} \times f_{leaf}\right] \quad (1)$$

where S is the weekly average *SWdown* (unit: W/m^2), LAI_4 (unit: m^2/m^2) is the *LAI* of leaf age Class 4, and C_1 and C_2 are empirical coefficients set to 35.0 (W/m^2) and 6.0 (unitless), respectively. They were calibrated against the observed seasonality of *LAI* cohorts (Wu et al., 2016). We use the root-mean-square error (RMSE) and Nash-Sutcliffe efficiency (NSE) metrics to evaluate the model for LAI_{young} and LAI_{old} (see section 4).

3.3.2.2. New Leaf Shedding Scheme

(1) Fixed observed date of canopy rejuvenation

In this first parameterization, we prescribe the dates of canopy rejuvenation when observed LAI_{young} reaches one third of the total *LAI*. These fixed empirical rejuvenation dates at the Southern Hemisphere BR-Sa1, BR-Sa3, and BR-Ma2 sites are close to the periods when *GPP* measurements from the eddy covariance instrumentation are observed to increase in the dry season, except for the Northern Hemisphere GF-Guy site which shows an opposite phase between *GPP* and LAI_{young} (see section 4). Such parameterization with fixed observed dates has little predictive value across sites, but it allows evaluating, on a first step, if the modified carbon allocation and leaf turnover modules correctly reproduce the seasonality of *LAI* and CO_2 and water fluxes.

After the canopy rejuvenation date, the shedding rate of old leaves is accelerated as follows:

$$\Delta B_i = B_i \times \min\left\{0.99, C_3 \times \min\left[0.99, \frac{\Delta t}{a_{crit}}\left(\frac{a_i}{a_{crit}}\right)^4\right]\right\} \quad (2)$$

where ΔB_i is the loss of biomass at each time step from age Class i, B_i is the leaf biomass of age Class i, Krinner et al. (2005) selected a 4 power law to ensure a rapid loss of leaf biomass when leaf age approaches the critical leaf age, C_3 (unitless) is an empirical coefficient set to 5.0 and calibrated using the seasonality of the measured total litterfall (see section 4). Outside the rejuvenation period, we keep the former leaf demography scheme.

(2) Variable dates of canopy rejuvenation

In a second parameterization, we introduced a more mechanistic description of the timing of leaf drop, testing different environmental factors to predict the canopy rejuvenation period. As opposed to using prescribed onset dates, a generic scheme brings a larger predictability for gridded simulations and temporal changes in canopy functioning. In order to find the most robust environmental trigger of canopy leaf rejuvenation for multiple-site applications, we tested three variables: precipitation, *SWdown*, and *VPD* (Figure 3)—as suggested by former studies (Bi et al., 2015; Xu et al., 2011; Saleska et al., 2016; Konings & Gentine, 2017; Tang & Dubayah, 2017; Giardina et al., 2018). We normalized these variables first by subtracting their mean annual value and then dividing by their standard deviation and then identified the dates at each site where these normalized variables cross over the zero line in both upward and downward directions. We use these dates to determine the leaf flushing and shedding in the improved ORCHIDEE model, respectively. Table 2 suggests that the precipitation, *SWdown* and *VPD*—determined starting of dry season is on average 3, 2, and 0.5 weeks later than the mean canopy rejuvenation start date determined by LAI_{young} at four eddy covariance flux tower sites in Amazonia. Therefore, the new ORCHIDEE version uses the upward crossover date of *VPD* is the best predictor of the observed canopy rejuvenation date in BR-Sa1, BR-Sa3, and BR-Ma2 sites. In contrast, at the GF-Guy site, the canopy rejuvenation period (i.e., *GPP* boost) happens during the wet season. Note that *VPD* has been proposed as a possible trigger of litterfall of old leaves (coincident with new leaves flushing) in tropical evergreen forests (Myers et al., 1998). We therefore chose the weekly *VPD* as a simple empirical trigger in the model to initiate the leaf shedding process and canopy rejuvenation for multiple-site simulations.

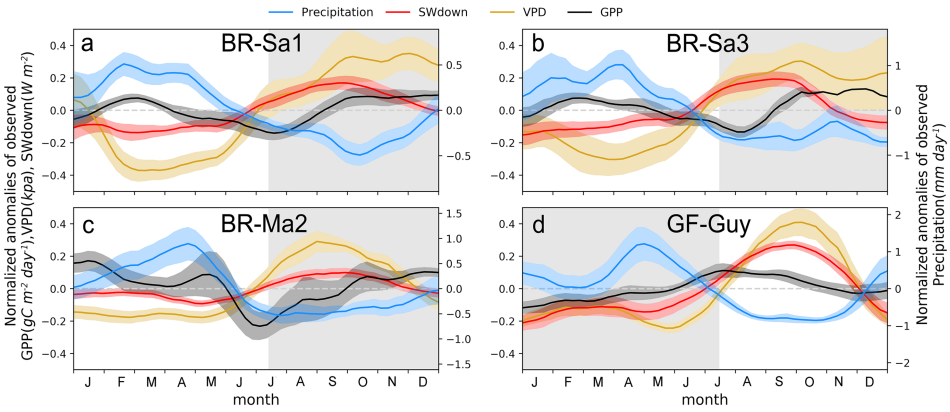

Figure 3. Mean seasonality of normalized precipitation (blue), *SWdown* (red), *VPD* (yellow) and *GPP* (black) for the (a) BR-Sa1, (b) BR-Sa3, (c) BR-Ma2, and (d) GF-Guy sites. The colored bands indicate the confidence intervals of 95%. The gray shading areas indicate the canopy rejuvenation periods.

The leaf shedding process that defines the biomass loss from the oldest leaf age class four was thus modified using weekly *VPD* as equation (3). For leaf age Classes 1 to 3, we kept the former leaf shedding scheme (section 3.2.2).

$$\Delta B_m = B_m \times \min\left\{0.99, (VPD_w/C_5)^{C_6} \times \min\left[0.99, \frac{\Delta t}{a_{crit}}\left(\frac{a_i}{a_{crit}}\right)^4\right]\right\} \quad (3)$$

where VPD_w indicates the weekly mean *VPD* (unit is kPa), and C_5 (kPa) and C_6 (unitless) are empirical coefficients set to 3.0 and 2.5 and calibrated to match the seasonality of the measured total litterfall (see section 4).

Based on the rationale that under the elevated *SWdown* in the dry season the shedding of older leaves (LAI_4) triggered by *VPD* results in more *NPP* being allocated to new leaves, the combination of a young canopy and stronger illumination is expected to increase the *GPP* in the dry season.

4. Results

4.1. Leaf Phenology Including *LAI*, Leaf Age, and Litterfall

To evaluate our model, we selected camera-based measurements, which provide a reliable observation of total *LAI* as well as *LAI* for different leaf age classes (cohorts), to calibrate the coeffecients of equation (1). The RMSE and NSE between modeled and observed LAI_{young} and LAI_{old} were on average equal to 0.57 (m^2/m^2) and 0.76, respectively, in comparison with the camera-based observations at the BR-Sa1 site. Figure 4 shows the seasonality of observed and ORCHIDEE-simulated *LAI* at the BR-Sa1 site. Clearly, the observed *LAI* of both new and old leaf age cohorts show a significant seasonality (Figure 4a). The LAI_{old} decreases and the LAI_{young} increases during the canopy rejuvenation period, but show the opposite behavior during the rest of the year. The former scheme in ORCHIDEE fails to reproduce any seasonality for the two canopy *LAI* cohorts (Figure 4b). The fixed-date (Figure 4c) and variable-date (Figure 4d) rejuvenation parameterizations both reasonably capture the observed seasonality of the *LAI* cohorts because the fraction of carbon allocated to new leaves is increased and shedding rate of old leaves is accelerated.

The old ORCHIDEE version shows no seasonality of leaf age and leaf photosynthetic efficiency in different age classes (Figures 5a and 5d). The fixed-date (Figure 4c) and variable-date (Figure 4d) rejuvenations, which differentiate the carbon allocation and leaf shedding processes between dry and wet seasons, successfully capture the seasonality of canopy leaf age (Figures 5b and 5c) and corresponding leaf efficiency in each leaf age class (Figures 5e and 5f). The RMSE and NSE of modeled versus observed *LAI* cohorts quantifies the improvement brought the new phenology scheme (Table S3). In general, the leaf age of young and old leaf

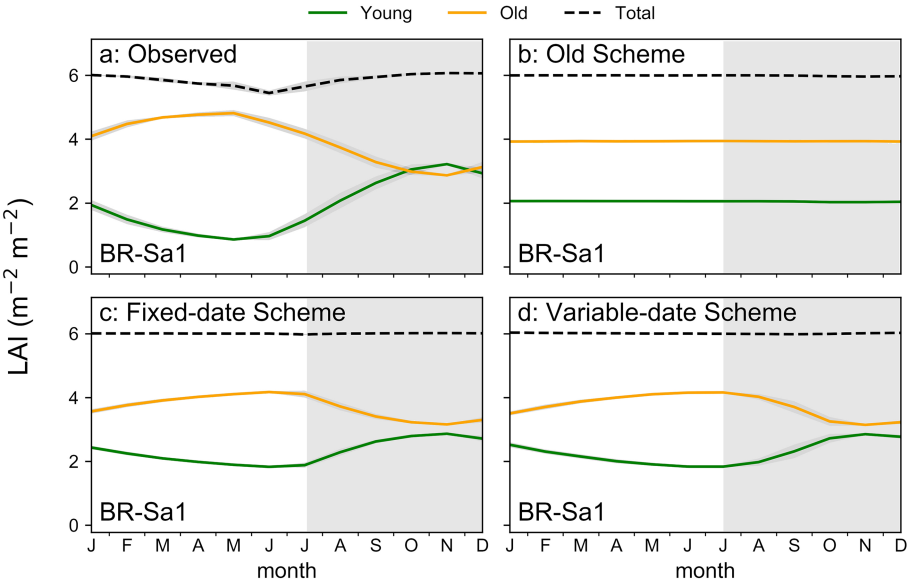

Figure 4. Mean seasonality of the canopy *LAI* cohorts in BR-Sa1 eddy covariance flux tower site. (a) Camera-observed; (b) old scheme; (c) fixed-date rejuvenation scheme; and (d) variable-date rejuvenation scheme. The camera-observed LAI_{young}: <6 months and LAI_{old}: ≥ 6 months. The modeled LAI_{young}: Class 1 and LAI_{old}: sum of Classes 2, 3, and 4. The gray shading areas indicate the canopy rejuvenation period.

cohorts both become older in the wet season but are younger in the dry season; the leaf photosynthetic efficiency shows as expected a trend opposite to the leaf age seasonality.

For the two improved litterfall schemes, the equations (2) and (3) yield an average RMSE and NSE of 0.44 (g C·m^{-2}·day^{-1}) and 0.39, and 0.32 (g C·m^{-2}·day^{-1}) and 0.49, respectively, calibrated using the data of all the four sites. As shown in Figure 6 (gray curves), the default canopy demography scheme produces little variability in the seasonal litterfall pattern at BR-Sa1 (NSE < −10; RMSE = 1.73 g C·m^{-2}·day^{-1}), BR-Sa3 (NSE < −10; RMSE = 0.38 g C·m^{-2}·day^{-1}), BR-Ma2 (NSE < −10; RMSE = 0.27 g C·m^{-2}·day^{-1}), and GF-Guy (NSE < −10; RMSE = 1.91 g C·m^{-2}·day^{-1}). By implementing the fixed-date rejuvenation parameterization the simulated seasonality of litterfall better coincides with that of observed litterfall at BR-Sa1 (NSE = −1.24; RMSE = 0.63 g C·m^{-2}·day^{-1}), BR-Sa3 (NSE = 0.2; RMSE = 0.51 g C·m^{-2}·day^{-1}), and BR-Ma2 (NSE = 0.59; RMSE = 0.17 g C·m^{-2}·day^{-1}), showing increased litterfall in the canopy rejuvenation season. By contrast, the fixed-

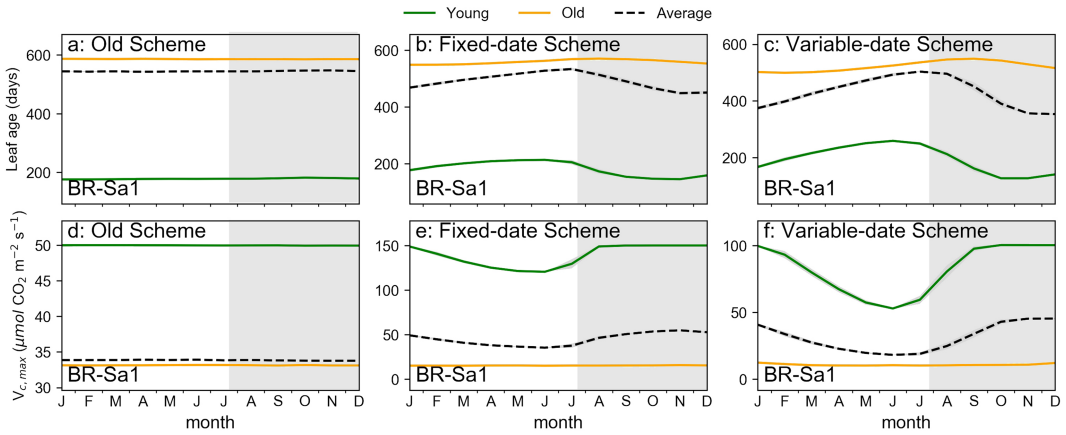

Figure 5. Mean seasonality of canopy leaf age and $V_{c,max}$ at the BR-Sa1 site. (a–c) The leaf age simulated by the old, fixed-date, and variable-date rejuvenation schemes, respectively; (d–f) the $V_{c,max}$ simulated by the old, fixed-date, and variable-date schemes, respectively. The gray shading areas indicate the canopy rejuvenation period.

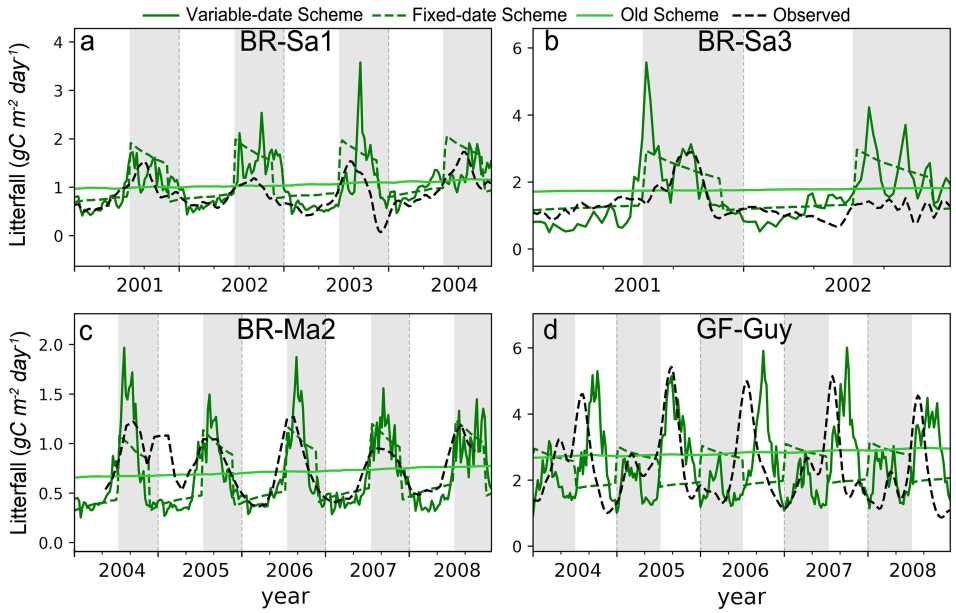

Figure 6. Seasonality of total litterfall at four eddy covariance flux tower sites. (a) BR-Sa1; (b) BR-Sa3; (c) BR-Ma2; (d) GF-Guy. The gray shading areas indicate the canopy rejuvenation periods.

date rejuvenation parameterization shows poor performances (NSE = −7.14; RMSE = 1.3 g C·m^{-2}·day^{-1}) in estimating the seasonality of litterfall at the GF-Guy site.

By using *VPD* to trigger rejuvenation in the variable-date rejuvenation parameterization, the model also captures the timing of litterfall, just before the seasonal maximum of *VPD* during the peak of the dry season (Figure 6, green curves). The RMSE and NSE of modeled litterfall are significantly improved at three sites: BR-Sa1 (NSE = 0.23; RMSE = 0.31 g C·m^{-2}·day^{-1}), BR-Sa3 (NSE = 0.53; RMSE = 0.47 g C·m^{-2}·day^{-1}), BR-Ma2 (NSE = 0.71; RMSE = 0.17 g C·m^{-2}·day^{-1}), and GF-Guy (NSE = 0.14; RMSE = 1.17 g C·m^{-2}·day^{-1}).

Multiple-site simulations (time period: 1990–2010) using the old scheme and the variable-date rejuvenation scheme were conducted to compare annual mean total litterfall with observations from 19 other sites in Amazonia (Chave et al., 2010) (Table S4 and Figure 7). In comparison with the old scheme (RMSE = 0.55 g C·m^{-2}·day^{-1}), the validation results were greatly improved by using the variable-date rejuvenation scheme (RMSE = 0.25 g C·m^{-2}·day^{-1}). The NSE of the variable-date scheme for litterfall shows improvements in modeling the litterfall seasonality as compared with the old scheme that has virtually no litter seasonality (Table S5). These results confirm that *VPD* is a possible precursor of litterfall in Amazonian forest, although we still lack a theoretical basis for the underlying processes.

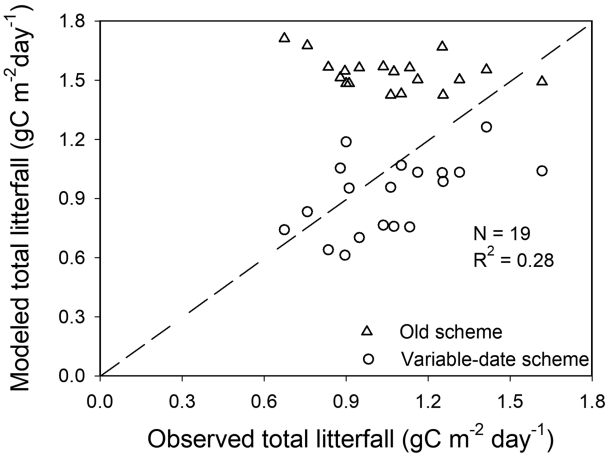

Figure 7. Scatterplot of observed against modeled annual mean total litterfall at 19 sites in the Amazonia.

4.2. Seasonality of the Carbon Allocation

The fractions of *NPP* allocated to leaves (f_{leaf}), roots (f_{root}), and sapwood (f_{sap}) vary seasonally in Amazonian evergreen forest (Da Silva et al., 2002; Metcalfe et al., 2008; Schöngart et al., 2002; Wagner et al., 2012). Figure 8 shows monthly means of f_{leaf}, f_{root}, and f_{sap} in Amazonian evergreen forest, averaged from the multiple-site observations of Doughty et al. (2015). The f_{leaf} varies positively with *SWdown* (Figure 2), while f_{root} and f_{sap} change in the opposite direction; this pattern is consistent with other observations in Amazonia (Da Silva et al., 2002; Metcalfe et al., 2008; Schöngart et al., 2002; Wagner et al., 2012). The standard allocation scheme of ORCHIDEE, as in most LSMs, showed little seasonality of f_{leaf}, f_{root}, and f_{sap} (Figure 8). Regulated by *SWdown*, the patterns of simulated f_{leaf}, f_{root}, and f_{sap} (solid curves, Figure 8) from the new allocation scheme

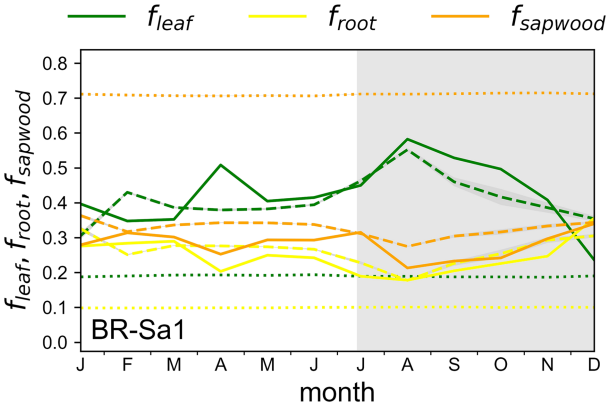

Figure 8. Fractions of carbon allocated to leaves (f_{leaf}), roots (f_{root}), and sapwood (f_{sap}) at BR-Sa1. (a) old scheme; (b) new scheme and field observations. Solid, dash and dot curves indicate the data from field observations, the variable-date scheme and the fixed-date scheme, respectively. The gray shading areas indicate the canopy rejuvenation period.

(equation (1)) agree better with the observed allocation (dash curves, Figure 8). The results, for which noticeably the NSEs of the variable-date scheme modeled allocation fractions against observations are all larger than 0 (Table S6), suggest that the seasonality of carbon allocation to different organs of trees, leaves, roots, and sapwood, is consistent with an initiation by the seasonality of incoming light (*SWdown*) conditions.

4.3. Seasonality of Carbon and Water Fluxes (i.e., Canopy-Scale *GPP* and *LE*)

Figure 9 shows the time series of *GPP* for the default canopy demography scheme, the fixed-date, variable-date rejuvenation parameterizations, and field measurements at the four eddy covariance sites (Table S5). The modeled *GPP* is improved by using the fixed-date rejuvenation scheme (BR-Sa1: RMSE = 0.65 g C·m^{-2}·day^{-1}, NSE = 0.23; BR-Sa3: RMSE = 0.58 g C·m^{-2}·day^{-1}, NSE = −1.45; BR-Ma2: RMSE = 1.55 g C·m^{-2}·day^{-1}, NSE < −10; GF-Guy: RMSE = 0.68 g C·m^{-2}·day^{-1}, NSE = −0.63) in comparison to the default scheme (BR-Sa1: RMSE = 0.77 g C·m^{-2}·day^{-1}, NSE = −8.65; BR-Sa3: RMSE = 0.59 g C·m^{-2}·day^{-1}, NSE < −10; BR-Ma2: RMSE = 2.08 g C·m^{-2}·day^{-1}, NSE < −10; GF-Guy: RMSE = 0.76 g C·m^{-2}·day^{-1}, NSE < −10). The variable-date rejuvenation parameterization also performs well in simulating the *GPP* seasonality at BR-Sa1, BR-Sa3, and BR-Ma2 (Table S5). However, the variable-date rejuvenation parameterization better captures the litterfall seasonality (Figure 6d) but fails to reproduce the *GPP* seasonality at the GF-Guy site (RMSE = 1.07 g C·m^{-2}·day^{-1}; NSE = −2.93). We suspect that the phase mismatch of the simulated *GPP* against observations at GF-Guy is related to the fact that this site has two dry-season periods and the rejuvenation period (Figure 3d) is not correctly captured by the proposed allocation scheme in equation (1).

We further evaluated the impacts of the fixed versus variable-date rejuvenation parameterization on the *LE* seasonality. For all the four sites, neither parameterization improves the simulations of *LE*, as compared with the default canopy demography scheme (Figure 10). The RMSE and NSE are shown in Table S5.

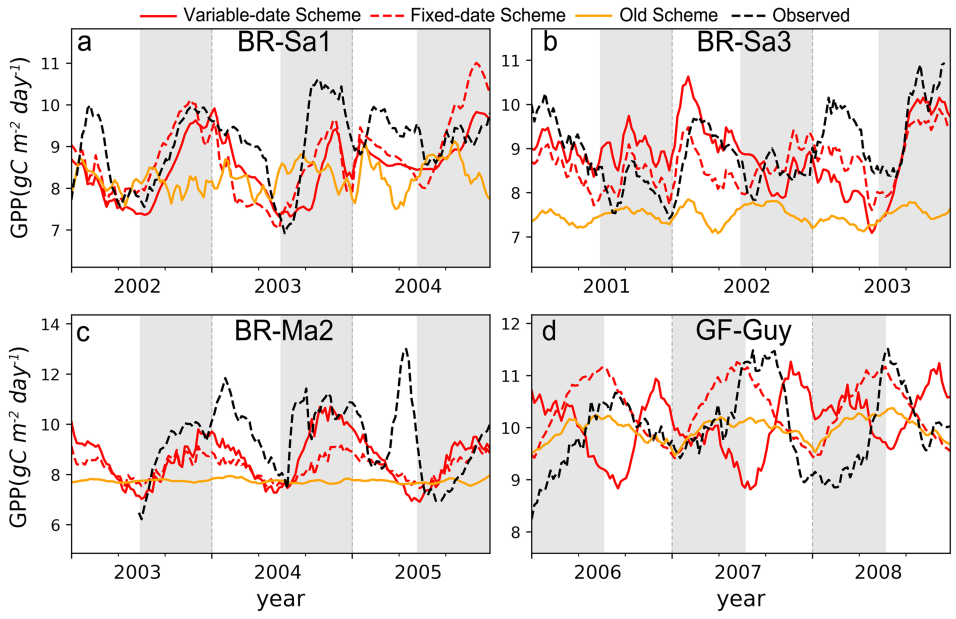

Figure 9. Seasonality of *GPP* at four eddy covariance flux tower sites. (a) BR-Sa1; (b) BR-Sa3; (c) BR-Ma2; (d) GF-Guy. The gray shading areas indicate the canopy rejuvenation periods.

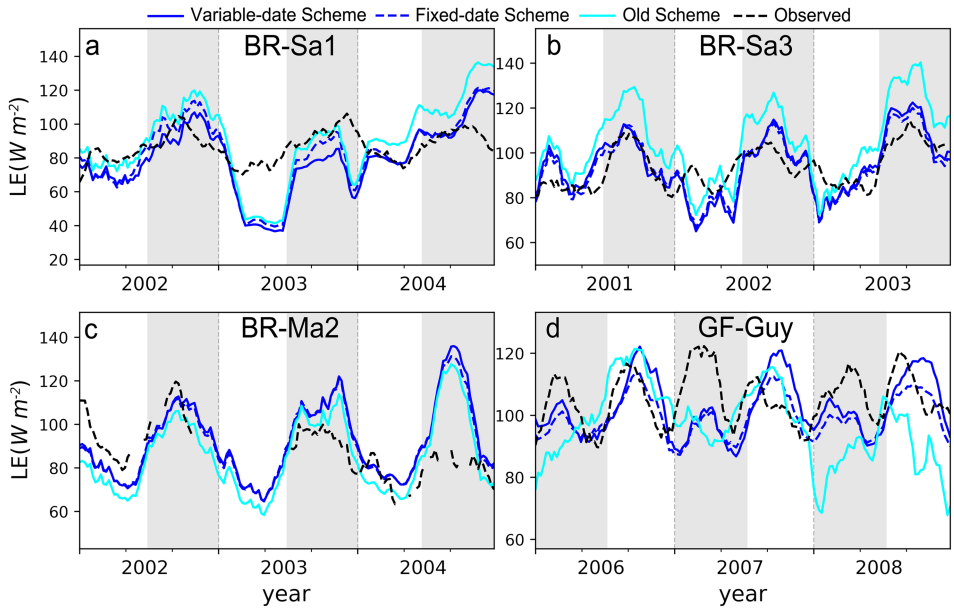

Figure 10. Seasonality of *LE* at four eddy covariance flux tower sites. (a) BR-Sa1; (b) BR-Sa3; (c) BR-Ma2; (d) GF-Guy. The gray shading areas indicate the canopy rejuvenation periods.

5. Discussion

5.1. The New Model With Environment-Driven Carbon Allocation and Litterfall Improves the Representation of Leaf Phenology

The existence of a single climatic variable precursor of canopy rejuvenation in tropical evergreen forests is a complex and debated issue as former studies have attributed canopy rejuvenation to diverse mechanisms (Saleska et al., 2003; Huete et al., 2006; Bi et al., 2015; Xu et al., 2015; Wu et al., 2016; Tang & Dubayah, 2017). Some satellite-based studies covering the entire Amazon basin have indicated that incoming light is empirically correlated with tropical leaf phenology (e.g., Guan et al., 2015). Some studies also suggest that it is not climate but biotic interactions between plants and herbivore population dynamics, or ontogenic processes that may trigger leaf renewal. Lopes et al. (2016) attributed the tropical leaf phenology to an evolutionary strategy to avoid predation and disease on vulnerable young leaves.

Peak litterfall at the maximum values of *VPD* during the early dry season (July–September) (Figure 6) suggests *VPD* as a possible major cause of leaf shedding in all the four tropical forests (Myers et al., 1998). In addition, our analysis indicates that the tropical forests constrain allocations to stems and roots (Metcalfe et al., 2008), and shift more carbon to growing new leaves at the beginning of the dry season (July–September) when the incoming *SWdown* is stronger (Bi et al., 2015; Xu et al., 2015; Huete et al., 2006; Wu et al., 2016). Coupling light-driven allocation with the new model gives a good representation of the flushing of new leaves at three out of the four sites (Figure 4a) and also improves the seasonality of carbon allocation to leaves, roots, and sapwoods (Figure 8). Data from three out of the four Amazonian sites analyzed here support the light-controlled leaf flushing hypothesis of Guan et al. (2015) and support the environment-controlled leaf phenology hypotheses. The underlying mechanisms are probably that the tropical evergreen forests of this study are not water limited (Guan et al., 2015), having evolved deep root systems giving access to deep soil moisture reservoir (Christoffersen et al., 2014; da Rocha et al., 2004; Oliveira et al., 2005), and the dry-season replacement of lower-$V_{c,max}$ old leaves with the newly mature leaves of higher $V_{c,max}$ might be a long-term evolutionary strategy to optimize the carbon gain (Xu et al., 2017). However, the opposite behavior of GF-Guy with respect to the other sites is not explained by the variable-date scheme, while the fixed-date simulations both correlate well with the site observations. It is probably because that our choice of climate triggers for the flushing of new leaves might not work at sites with two dry-season periods. It is also worth noting that the simulated canopy rejuvenation starts around six weeks later as compared to the BR-Sa1 site: the decrease of the old class (orange curve) and the increase of the young one (green curve) in modeled

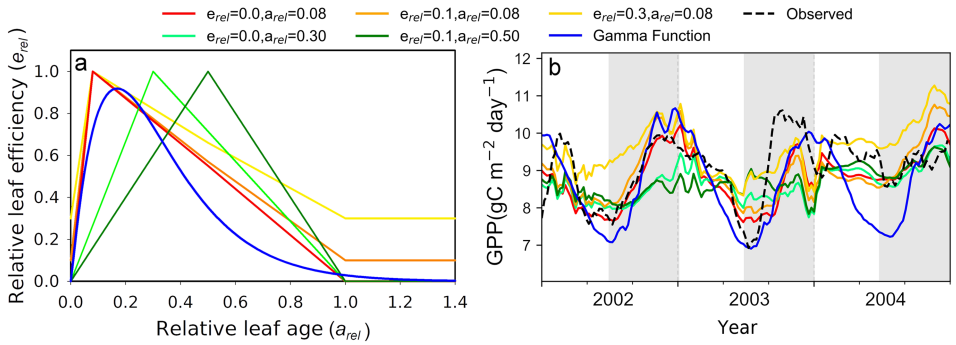

Figure 11. GPP seasonality for different minimums eref (red: 0.0; light red: 0.1; yellow: 0.3) at acrit , and for different aref(red: 0.08; light green: 0.3; green: 0.5) at the maximum eref. (a) erel as a function of arel ; (b) Simulated GPP seasonality at the BR-Sa1 site. The grey shading areas indicate the canopy rejuvenation period.

panels (Figures 4c and 4d) both lag the observed classes (Figure 4a). Further studies are planned to reduce this time-lag in.

The consistent relationships between the phenology of new leaf production and old leaf shedding with environmental drivers across the four Amazonian evergreen forests spanning a large rainfall gradient and having different species compositions bring new insight into the probably different mechanisms involved in new leaf flushing allocation and old leaf shedding in response to environment changes. These early results suggest great potential to take advantage of relationships between environmental forcing and leaf phenology to improve model performance over large spatial and temporal scales in Amazonia.

5.2. The New Phenology With Ontogeny-Associated PC Improves the Simulation of Carbon Seasonality

Introducing a new representation of the leaf phenology greatly improves the model's simulation of carbon and water cycles in Amazonian evergreen forest. During the rejuvenation period, the *GPP* is increased by 0 %, 2%, 0%, and 3% for the BR-Sa1, BR-Sa3, BR-Ma2, and GF-Guy sites, respectively, using the old scheme; by 15%, 8%, 7%, and 8% for the BR-Sa1, BR-Sa3, BR-Ma2, and GF-Guy sites, respectively, using the fixed-date scheme; by 9%, 4%, 9%, and 5% for the BR-Sa1, BR-Sa3, BR-Ma2, and GF-Guy sites, respectively, using the variable-date scheme (Figure S5).

The leaf phenology, particularly seasonal variation in leaf-age-dependent $V_{c,max}$, dominates the representations of carbon and water flux variability in the improved ORCHIDEE model. The results agree with previous studies inferred from field-observations of leaf/branch physiology (Albert et al., 2018), ecosystem-scale measurements of canopy $V_{c,max}$ and *GPP* dynamics (Wu et al., 2016), as well as the modeling results from both a big-leaf light-use-efficiency model (Wu, Guan, et al., 2017) and a more complex two-fraction (sun/shade), two-layer canopy model (Wu et al., 2017).

We further tested the sensitivity of the *GPP* seasonality to changes in the minimum leaf efficiency (red: $e_{ref} = 0.0$; light red: $e_{ref} = 0.1$; yellow: $e_{ref} = 0.3$) at a_{crit}, and to changes of a_{ref} (light green: $a_{ref} = 0.3$; green: $a_{ref} = 0.5$) at the maximum e_{ref}. (Figure 11a). Results show that the minimum *GPP* values over the year increase from 7.8 to 8.7 g C·m^{-2}·day^{-1} as the minimum e_{ref} at a_{crit} increases from 0.0 to 0.3. The maximum *GPP* values over the year decrease from 10.0 to 9.0 g C·m^{-2}·day^{-1} as the a_{ref} at maximum e_{crit} increases from 0.08 to 0.5 (Figure 11b). The amplitude of the *GPP* seasonality depends on the values of the minimum e_{ref} at a_{crit} and values of a_{ref} at maximum e_{crit}. In comparison, using a gamma function to fit the decrease of V_{cmax} with age instead of a linear function (Figure 11), the fixed-date scheme also gives robust performances in simulating the *GPP* seasonality (RMSE = 1.11 g C·m^{-2}·day^{-1}; NSE = 0.04; Table S7).

Note that some studies used alternative methods—variable *LAI* and constant leaf traits ($V_{c,max}$) as inputs (Fisher et al., 2007). However, Wu et al. (2016) observed very slight variations of total *LAI* (seasonal variability <0.5 m^2/m^2) at both BR-Sa1 and BR-Sa3 sites but an increase of ecosystem PC with light during the dry season (Figure 1 in Wu et al., 2016). Our results have similar seasonality of $V_{c,max}$ (Figure 5f). Therefore,

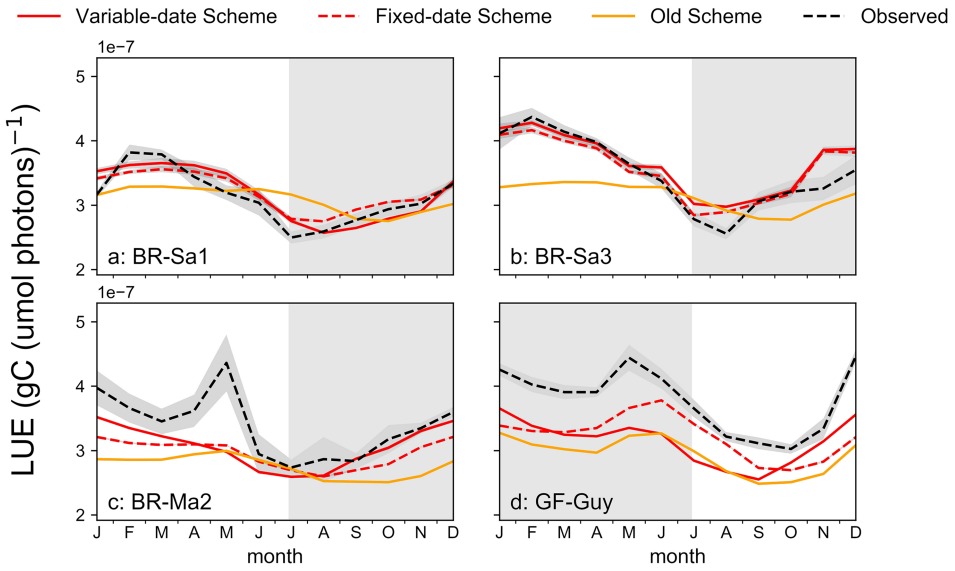

Figure 12. Seasonality of LUE at four eddy-covariance flux tower sites. (a)BR-Sa1; (b) BR-Sa3; (c) BR-Ma2; (d) GF-Guy. The grey shading areas indicate the canopy rejuvenation periods.

although controversial, we are more convinced that the $V_{c,max}$ variability, which influences the turnover rate from new grown leaves to mature leaves and the deactivation speed of leaf vitality, along with the leaf aging from mature leaves to old leaves, are the key parameters influencing the seasonal variation of *GPP* in Amazonian evergreen forest. To test the robustness of the new scheme, we made a regional simulation across the whole Amazonian evergreen forests. Preliminary results suggest that at this larger spatial scale the *GPP* seasonality is also improved when compared against satellite *GPP* proxies (Figure S6). Further work will address spatial patterns of the *GPP* seasonality across the Amazon.

Our simulation results highlight the importance of having leaf-age-dependent $V_{c,max}$ controlling the canopy photosynthesis in LSMs, if we are to accurately represent the *GPP* seasonal cycle. Most LSMs need further improvements in this respect. However, the optimal curve used to adjust the $V_{c,max}$-leaf age relationship needs to be discussed and validated by more field observations. It is to be noted that leaf aging may impact not only on the PC but more broadly on the leaf metabolism including leaf respiration, which will in turn affect *GPP*. More leaf-level studies are needed to address this issue.

5.3. The New Phenology With a Younger Canopy Impacts on Light Use Efficiency and Soil Moisture

Wu et al. (2016) observed that an accelerated litterfall of old leaves and the growth of new leaves at the beginning of dry season shifts the canopy toward younger leaves, which explained a ~27% seasonal increase in photosynthetic efficiency, defined by the age classes and associated age-dependent light use efficiency (LUE) parameters. Young leaves have indeed a larger LUE (Doughty & Goulden, 2008). Our scheme (Figure 12) captures such an increased LUE in the dry-season period (Table S8).

Soil moisture deficit is another key factor decreasing the soil water potential and inducing vegetation water stress (Manoli et al., 2018). This process is imperfectly understood for evergreen forests (Manoli et al., 2018) as it involves the resistance of water transfer from soil to roots and xylem transport driven by leaf water potential and stem conductivity. However, as most Amazonian humid forests are not usually water limited, there is in general no severe soil water stress on canopy photosynthesis, except in the southern part of the Amazonia (Guan et al., 2015). That is probably why decreasing soil moisture does not always lead to reduced *GPP* both in the data and our model results. We found than a younger canopy uses more soil moisture to sustain the increased *GPP* in the dry season period (Figure S7). But soil moisture can become limiting like in drought events in 2001 and 2002 at BR-Sa3 (Baker et al., 2008; Nepstad et al., 2007). That is why for instance the *GPP* seasonality at BR-Sa3 has a sudden drop in the dry season, a response different from the one at the BR-Sa1 site, even though the two sites are nearby. Effects of increased atmospheric stress

(VPD) (Figure S8) might also impact *GPP* on shorter time scales. The observed and modeled responses of *GPP* to PAR (Figures S9 and S10) are in qualitative agreement, and both show a positive response of *GPP* to light in the dry season. However, during drought events at BR-Sa3 both simulated and observed *GPP* decrease as PAR increases due to water stress. The model cannot correctly reproduce the observed relationship between *GPP* and PAR at GF-Guy (Figure S10d), since it misses the *GPP* seasonality.

6. Conclusions

This study proposes a mechanistic climate-triggered leaf age demography model in combination with ontogeny-dependent leaf PC changes. The new leaf age demography evolution scheme performs reasonably well in modeling the leaf phenology (*LAI* cohorts, leaf age) at multiple forest sites (BR-Sa1, BR-Sa3, BR-Ma2, and GF-Guy) across Amazonia. The new model scheme leads to improved seasonality of simulated carbon and water fluxes (*GPP*, *LE*). The higher proportion of young leaves with greater photosynthetic efficiency is the major cause boosting *GPP* of tropical evergreen forests during the dry season. The new model, coupled with a priority allocation to young leaves at high sunlight in the early dry season, additionally matches the observed seasonality of carbon allocation and leaf shedding processes (allocation fractions, litterfall). This supports the roles of *SWdown* and *VPD* as climate drivers that control canopy leaf flushing and shedding processes of Amazonian evergreen forests.

The proposed model provides a feasible implementation for gridded simulations of carbon and water fluxes from Amazonia. However, the new scheme is unable to trigger the *GPP* seasonality where the leaf flushing happens in the wet season when there is adequate water but *SWdown* is smaller, like the situation at the GF-Guy site. It still remains to be tested if the new scheme holds also true in other LSMs, provided that, like ORCHIDEE, those models include leaf age cohorts.

Acknowledgments
We thank the Editor and the anonymous reviewers for their valuable comments and thank Dan Zhu, Chunjing Qiu, Ye Huang, and the MICT group for their help and discussions on the use of the ORCHIDEE model. Data availability: https://zenodo.org/record/3529310#.XcFfK3aASZR (DOI: 10.5281/zenodo.3529310). This research was financed by the Belgian Science Policy Office (Belspo)—Research Programme for Earth Observation, STEREO III, Contract SR/00/334 (ECOPROPHET project), and CLIMAX Climate Services Through Knowledge Co-Production: A Euro-South American Initiative For Strengthening Societal Adaptation Response to Extreme Events cofunded by the ANR in the Belmont Forum/JPI-Climate—Climate Services CRA 201. X. C. was supported by the National Natural Science Foundation of China (Grants 31500357 and 41401055). J. W. was supported by the United States Department of Energy Contract DE-SC0012704 to Brookhaven National Laboratory. This work used the eddy covariance data acquired and shared by the FLUXNET community, mainly from AmeriFlux. The ERA-Interim reanalysis data are provided by ECMWF and processed by LSCE. The FLUXNET eddy covariance data processing and harmonization was carried out by the European Fluxes Database Cluster, AmeriFlux Management Project, and Fluxdata project of FLUXNET, with the support of CDIAC and ICOS Ecosystem Thematic Center, and the OzFlux, ChinaFlux and AsiaFlux offices.

References

Albert, L. P., Wu, J., Prohaska, N., de Camargo, P. B., Huxman, T. E., Tribuzy, E. S., et al. (2018). Age-dependent leaf physiology and consequences for crown-scale carbon uptake during the dry season in an Amazon evergreen forest. *New Phytologist*, *219*(3), 870–884. https://doi.org/10.1111/nph.15056

Araújo, A. C., Nobre, A. D., Kruijt, B., Elbers, J. A., Dallarosa, R., Stefani, P., et al. (2002). Comparative measurements of carbon dioxide fluxes from two nearby towers in a central Amazonian rainforest: The Manaus LBA site. *Journal of Geophysical Research*, *107*(D20), 8090. https://doi.org/10.1029/2001JD000676

Asner, G. P., & Alencar, A. (2010). Drought impacts on the Amazon forest: The remote sensing perspective. *New Pytologist*, *187*(3), 569–578.

Baker, I. T., Prihodko, L., Denning, A. S., Goulden, M., Miller, S., & Da Rocha, H. R. (2008). Seasonal drought stress in the Amazon: Reconciling models and observations. *Journal of Geophysical Research*, *113*, G00B01. https://doi.org/10.1029/2007JG000644

Beer, C., Reichstein, M., Tomelleri, E., Ciais, P., Jung, M., Carvalhais, N., et al. (2010). Terrestrial gross carbon dioxide uptake: Global distribution and covariation with climate. *Science*, *329*(5993), 834–838. https://doi.org/10.1126/science.1184984

Bi, J., Knyazikhin, Y., Choi, S., Park, T., Barichivich, J., Ciais, P., et al. (2015). Sunlight mediated seasonality in canopy structure and photosynthetic activity of Amazonian rainforests. *Environmental Research Letters*, *10*(6), 064014.

Bonal, D., Bosc, A., Ponton, S., Goret, J. Y., Burban, B., Gross, P., et al. (2008). Impact of severe dry season on net ecosystem exchange in the neotropical rainforest of French Guiana. *Global Change Biology*, *14*(8), 1917–1933.

Brando, P. M., Goetz, S. J., Baccini, A., Nepstad, D. C., Beck, P. S., & Christman, M. C. (2010). Seasonal and interannual variability of climate and vegetation indices across the Amazon. *Proceedings of the National Academy of Sciences of the United States of America*, *107*(33), 14685–14690. https://doi.org/10.1073/pnas.0908741107

Chave, J., Navarrete, D., Almeida, S., Alvarez, E., Aragao, L. E. O. C., Bonal, D., et al. (2010). Regional and seasonal patterns of litterfall in tropical South America. *Biogeosciences*, *7*(1), 43–55.

Christoffersen, B. O., Restrepo-Coupe, N., Arain, M. A., Baker, I. T., Cestaro, B. P., Ciais, P., et al. (2014). Mechanisms of water supply and vegetation demand govern the seasonality and magnitude of evapotranspiration in Amazonia and Cerrado. *Agricultural and Forest Meteorology*, *191*, 33–50.

Da Rocha, H. R., Goulden, M. L., Miller, S. D., Menton, M. C., Pinto, L. D., de Freitas, H. C., & de Silva Figueira, A. M. (2004). Seasonality of water and heat fluxes over a tropical forest in eastern Amazonia. *Ecological Aplications*, *14*(sp4), 22–32.

Da Silva, R. P., dos Santos, J., Tribuzy, E. S., Chambers, J. Q., Nakamura, S., & Higuchi, N. (2002). Diameter increment and growth patterns for individual tree growing in Central Amazon, Brazil. *Forest Ecology and Management*, *166*(1-3), 295–301.

Davidson, E. A., de Araújo, A. C., Artaxo, P., Balch, J. K., Brown, I. F., Bustamante, M. M., et al. (2012). The Amazon basin in transition. *Nature*, *481*(7381), 321–328. https://doi.org/10.1038/nature10717

De Weirdt, M., Verbeeck, H., Maignan, F., Peylin, P., Poulter, B., Bonal, D., et al. (2012). Seasonal leaf dynamics for tropical evergreen forests in a process-based global ecosystem model. *Geoscientific Model Development*, *5*(5), 1091–1108.

Detto, M., Wright, S. J., Calderón, O., & Muller-Landau, H. C. (2018). Resource acquisition and reproductive strategies of tropical forest in response to the El Niño–Southern Oscillation. *Nature Communications*, *9*(1), 913. https://doi.org/10.1038/s41467-018-03306-9

Doughty, C. E., & Goulden, M. L. (2008). Are tropical forests near a high temperature threshold? *Journal of Geophysical Research*, *113*, G00B07. https://doi.org/10.1029/2007JG000632

Doughty, C. E., Metcalfe, D. B., Girardin, C. A. J., Amézquita, F. F., Cabrera, D. G., Huasco, W. H., et al. (2015). Drought impact on forest carbon dynamics and fluxes in Amazonia. *Nature*, *519*(7541), 78.

Farquhar, G. D., von Caemmerer, S. V., & Berry, J. A. (1980). A biochemical model of photosynthetic CO_2 assimilation in leaves of C 3 species. *Planta*, *149*(1), 78–90.
Fisher, R. A., Williams, M., Da Costa, A. L., Malhi, Y., Da Costa, R. F., Almeida, S., & Meir, P. (2007). The response of an Eastern Amazonian rain forest to drought stress: results and modelling analyses from a throughfall exclusion experiment. *Global Change Biology*, *13*(11), 2361–2378.
Fu, R., Yin, L., Li, W., Arias, P. A., Dickinson, R. E., Huang, L., et al. (2013). Increased dry-season length over southern Amazonia in recent decades and its implication for future climate projection. *Proceedings of the National Academy of Sciences of the United States of America*, *110*(45), 18110–18115. https://doi.org/10.1073/pnas.1302584110
Giardina, F., Konings, A. G., Kennedy, D., Alemohammad, S. H., Oliveira, R. S., Uriarte, M., & Gentine, P. (2018). Tall Amazonian forests are less sensitive to precipitation variability. *Nature Geoscience*, *11*(6), 405–409.
Guan, K., Pan, M., Li, H., Wolf, A., Wu, J., Medvigy, D., et al. (2015). Photosynthetic seasonality of global tropical forests constrained by hydroclimate. *Nature Geoscience*, *8*(4), 284–289.
Guimberteau, M., Ciais, P., Ducharne, A., Boisier, J. P., Aguiar, A. P. D., Biemans, H., et al. (2017). Impacts of future deforestation and climate change on the hydrology of the Amazon Basin: A multi-model analysis with a new set of land-cover change scenarios. *Hydrology and Earth System Sciences*, *21*(3), 1455.
Guimberteau, M., Zhu, D., Maignan, F., Huang, Y., Chao, Y., Dantec-Nédélec, S., et al. (2018). ORCHIDEE-MICT (v8. 4.1), a land surface model for the high latitudes: Model description and validation. *Geoscientific Model Development*, *11*(1), 121–163.
He, L., Chen, J. M., Liu, J., Mo, G., & Joiner, J. (2017). Angular normalization of gome-2 sun-induced chlorophyll fluorescence observation as a better proxy of vegetation productivity. *Geophysical Research Letters*, *44*, 5691–5699. https://doi.org/10.1002/2017GL073708
Huete, A. R., Didan, K., Shimabukuro, Y. E., Ratana, P., Saleska, S. R., Hutyra, L. R., et al. (2006). Amazon rainforests green-up with sunlight in dry season. *Geophysical Research Letters*, *33*, L06405. https://doi.org/10.1029/2005GL025583
Huntingford, C., Zelazowski, P., Galbraith, D., Mercado, L. M., Sitch, S., Fisher, R., et al. (2013). Simulated resilience of tropical rainforests to CO_2-induced climate change. *Nature Geoscience*, *6*(4), 268–273.
Hutyra, L. R., Munger, J. W., Saleska, S. R., Gottlieb, E., Daube, B. C., Dunn, A. L., et al. (2007). Seasonal controls on the exchange of carbon and water in an Amazonian rain forest. *Journal of Geophysical Research*, *112*, G03008. https://doi.org/10.1029/2006JG000365
Ishida, A., & Toma, T. (1999). Limitation of leaf carbon gain by stomatal and photochemical processes in the top canopy of Macaranga conifera, a tropical pioneer tree. *Tree Physiology*, *19*(7), 467–473.
Keller, M., Palace, M., & Hurtt, G. (2001). Biomass estimation in the Tapajos National Forest, Brazil: Examination of sampling and allometric uncertainties. *Forest Ecology and Management*, *154*(3), 371–382.
Konings, A. G., & Gentine, P. (2017). Global variations in ecosystem-scale isohydricity. *Global Change Biology*, *23*(2), 891–905. https://doi.org/10.1111/gcb.13389
Krinner, G., Viovy, N., de Noblet-Ducoudré, N., Ogée, J., Polcher, J., Friedlingstein, P., et al. (2005). A dynamic global vegetation model for studies of the coupled atmosphere-biosphere system. *Global Biogeochemical Cycles*, *19*, GB1015. https://doi.org/10.1029/2003GB002199
Lardy, R., Bellocchi, G., & Soussana, J. F. (2011). A new method to determine soil organic carbon equilibrium. *Environmental modelling & Software*, *26*(12), 1759–1763.
Lee, J. E., Frankenberg, C., van der Tol, C., Berry, J. A., Guanter, L., Boyce, C. K., et al. (2013). Forest productivity and water stress in Amazonia: Observations from GOSAT chlorophyll fluorescence. *Proceedings of the Royal Society of London B: Biological Sciences*, *280*(1761).
Le Quéré, C. L., Andrew, R. M., Friedlingstein, P., Sitch, S., Pongratz, J., Manning, A. C., et al. (2018). Global carbon budget 2017. *Journal of Earth System Science Data*, *10*, 405–448. https://doi.org/10.5194/essd-10-405-2018
Lopes, A. P., Nelson, B. W., Wu, J., de Alencastro Graça, P. M. L., Tavares, J. V., Prohaska, N., et al. (2016). Leaf flush drives dry season green-up of the Central Amazon. *Remote Sensing of Environment*, *182*, 90–98.
Malhi, Y., Aragao, L. E. O., Metcalfe, D. B., Paiva, R., Quesada, C. A., Almeida, S., et al. (2009). Comprehensive assessment of carbon productivity, allocation and storage in three Amazonian forests. *Global Change Biology*, *15*(5), 1255–1274.
Manoli, G., Ivanov, V. Y., & Fatichi, S. (2018). Dry season greening and water stress in Amazonia: The role of modeling leaf phenology. *Journal of Geophysical Research: Biogeosciences*, *123*, 1909–1926. https://doi.org/10.1029/2017JG004282
Metcalfe, D. B., Meir, P., Aragão, L. E. O. C., da Costa, A. C. L., Braga, A. P., Gonçalves, P. H. L., et al. (2008). The effects of water availability on root growth and morphology in an Amazon rainforest. *Plant and Soil*, *311*(1-2), 189–199.
Misson, L., Tu, K. P., Boniello, R. A., & Goldstein, A. H. (2006). Seasonality of photosynthetic parameters in a multi-specific and vertically complex forest ecosystem in the Sierra Nevada of California. *Tree Physiology*, *26*(6), 729–741. https://doi.org/10.1093/treephys/26.6.729
Morton, D. C., Nagol, J., Carabajal, C. C., Rosette, J., Palace, M., Cook, B. D., et al. (2014). Amazon forests maintain consistent canopy structure and greenness during the dry season. *Nature*, *506*(7487), 221–224. https://doi.org/10.1038/nature13006
Myers, B. A., Williams, R. J., Fordyce, I., Duff, G. A., & Eamus, D. (1998). Does irrigation affect leaf phenology in deciduous and evergreen trees of the savannas of northern Australia? *Austral Ecology*, *23*(4), 329–339.
Nepstad, D. C., Tohver, I. M., Ray, D., Moutinho, P., & Cardinot, G. (2007). Mortality of large trees and lianas following experimental drought in an Amazon forest. *Ecology*, *88*(9), 2259–2269. https://doi.org/10.1890/06-1046.1
Niinemets, Ü., Sun, Z., & Talts, E. (2015). Controls of the quantum yield and saturation light of isoprene emission in different-aged aspen leaves. *Plant, cell & environment*, *38*(12), 2707–2720.
Oliveira, R. S., Bezerra, L., Davidson, E. A., Pinto, F., Klink, C. A., Nepstad, D. C., & Moreira, A. (2005). Deep root function in soil water dynamics in cerrado savannas of central Brazil. *Functional Ecology*, *19*(4), 574–581.
Pan, Y., Birdsey, R. A., Fang, J., Houghton, R., Kauppi, P. E., Kurz, W. A., et al. (2011). A large and persistent carbon sink in the world's forests. *Science*, *333*(6045), 988–993. https://doi.org/10.1126/science.1201609
Papale, D., Reichstein, M., Aubinet, M., Canfora, E., Bernhofer, C., Kutsch, W., et al. (2006). Towards a standardized processing of Net Ecosystem Exchange measured with eddy covariance technique: Algorithms and uncertainty estimation. *Biogeosciences*, *3*(4), 571–583.
Peñuelas, J., & Filella, I. (2009). Phenology feedbacks on climate change. *Science*, *324*(5929), 887–888.
Peng, S., Ciais, P., Chevallier, F., Peylin, P., Cadule, P., Sitch, S., et al. (2015). Benchmarking the seasonal cycle of CO_2 fluxes simulated by terrestrial ecosystem models. *Global Biogeochemical Cycles*, *29*(1), 46–64.
Poorter, H., Niklas, K. J., Reich, P. B., Oleksyn, J., Poot, P., & Mommer, L. (2012). Biomass allocation to leaves, stems and roots: Meta-analyses of interspecific variation and environmental control. *New Phytologist*, *193*(1), 30–50. https://doi.org/10.1111/j.1469-8137.2011.03952.x
Potter, C., Genovese, V. B., Klooster, S., Bobo, M., & Torregrosa, A. (2001). Biomass burning losses of carbon estimated from ecosystem modeling and satellite data analysis for the Brazilian Amazon region. *Atmospheric Environment*, *35*(10), 1773–1781.

Poulter, B., Heyder, U., & Cramer, W. (2009). Modeling the sensitivity of the seasonal cycle of GPP to dynamic LAI and soil depths in tropical rainforests. *Ecosystems*, *12*(4), 517–533.

Restrepo-Coupe, N., da Rocha, H. R., Hutyra, L. R., da Araujo, A. C., Borma, L. S., Christoffersen, B., et al. (2013). What drives the seasonality of photosynthesis across the Amazon basin? A cross-site analysis of eddy flux tower measurements from the Brasil flux network. *Agricultural and Forest Meteorology*, *182*, 128–144.

Restrepo-Coupe, N., Huete, A., Davies, K., Cleverly, J., Beringer, J., Eamus, D., et al. (2016). MODIS vegetation products as proxies of photosynthetic potential along a gradient of meteorologically and biologically driven ecosystem productivity. *Biogeosciences*, *13*(19), 5587–5608.

Restrepo-Coupe, N., Levine, N. M., Christoffersen, B. O., Albert, L. P., Wu, J., Costa, M. H., et al. (2017). Do dynamic global vegetation models capture the seasonality of carbon fluxes in the Amazon basin? A data-model intercomparison. *Global Change Biology*, *23*(1), 191–208. https://doi.org/10.1111/gcb.13442

Rice, A. H., Pyle, E. H., Saleska, S. R., Hutyra, L., Palace, M., Keller, M., et al. (2004). Carbon balance and vegetation dynamics in an old-growth Amazonian forest. *Ecological Applications*, *14*(sp4), 55–71.

Rödig, E., Cuntz, M., Rammig, A., Fischer, R., Taubert, F., & Huth, A. (2018). The importance of forest structure for carbon fluxes of the Amazon rainforest. *Environmental Research Letters*, *13*(5), 054013.

Saleska, S. R., Miller, S. D., Matross, D. M., Goulden, M. L., Wofsy, S. C., da Rocha, H. R., et al. (2003). Carbon in Amazon forests: Unexpected seasonal fluxes and disturbance-induced losses. *Science*, *302*(5650), 1554–1557.

Saleska, S. R., Wu, J., Guan, K., Araujo, A. C., Huete, A., Nobre, A. D., & Restrepo-Coupe, N. (2016). Dry-season greening of Amazon forests. *Nature*, *531*(7594), E4.

Schimel, D., Pavlick, R., Fisher, J. B., Asner, G. P., Saatchi, S., Townsend, P., et al. (2015). Observing terrestrial ecosystems and the carbon cycle from space. *Global Change Biology*, *21*(5), 1762–1776. https://doi.org/10.1111/gcb.12822

Schoettle, A. W., & Fahey, T. J. (1994). Foliage and fine root longevity of pines. *Ecological Bulletins*, *43*, 136–153.

Schöngart, J., Piedade, M. T. F., Ludwigshausen, S., Horna, V., & Worbes, M. (2002). Phenology and stem-growth periodicity of tree species in Amazonian floodplain forests. *Journal of Tropical Ecology*, *18*(4), 581–597.

Sitch, S., Friedlingstein, P., Gruber, N., Jones, S. D., Murray-Tortarolo, G., Ahlström, A., et al. (2013). Trends and drivers of regional sources and sinks of carbon dioxide over the past two decades. *Biogeosciences Discussions*, *10*, 20,113–20,177.

Tang, H., & Dubayah, R. (2017). Light-driven growth in Amazon evergreen forests explained by seasonal variations of vertical canopy structure. *Proceedings of the National Academy of Sciences of the United States of America*, *114*(10), 2640–2644. https://doi.org/10.1073/pnas.1616943114

Traore, A. K., Ciais, P., Vuichard, N., Poulter, B., Viovy, N., Guimberteau, M., & Fisher, J. B. (2014). Evaluation of the ORCHIDEE ecosystem model over Africa against 25 years of satellite-based water and carbon measurements. *Journal of Geophysical Research: Biogeosciences*, *119*, 1554–1575. https://doi.org/10.1002/2014JG002638

Wagner, F., Rossi, V., Stahl, C., Bonal, D., & Herault, B. (2012). Water availability is the main climate driver of neotropical tree growth. *PLoS One*, *7*(4), e34074. https://doi.org/10.1371/journal.pone.0034074

Wright, J. S., Fu, R., Worden, J. R., Chakraborty, S., Clinton, N. E., Risi, C., et al. (2017). Rainforest-initiated wet season onset over the southern Amazon. *Proceedings of the National Academy of Sciences of the United States of America*, *114*(32), 8481–8486.

Wu, J., Albert, L. P., Lopes, A. P., Restrepo-Coupe, N., Hayek, M., Wiedemann, K. T., et al. (2016). Leaf development and demography explain photosynthetic seasonality in Amazon evergreen forests. *Science*, *351*(6276), 972–976.

Wu, J., Guan, K., Hayek, M., Restrepo-Coupe, N., Wiedemann, K. T., Xu, X., et al. (2017). Partitioning controls on Amazon forest photosynthesis between environmental and biotic factors at hourly to interannual timescales. *Global Change Biology*, *23*(3), 1240–1257.

Wu, J., Kobayashi, H., Stark, S. C., Meng, R., Guan, K., Tran, N. N., et al. (2018). Biological processes dominate seasonality of remotely sensed canopy greenness in an Amazon evergreen forest. *New Phytologist*, *217*(4), 1507–1520. https://doi.org/10.1111/nph.14939

Wu, J., Serbin, S. P., Xu, X., Albert, L. P., Chen, M., Meng, R., et al. (2017). The phenology of leaf quality and its within-canopy variation is essential for accurate modeling of photosynthesis in tropical evergreen forests. *Global Change Biology*, *23*(11), 4814–4827. https://doi.org/10.1111/gcb.13725

Xu, X., Medvigy, D., Joseph, W. S., Kitajima, K., Wu, J., Albert, L. P., et al. (2017). Variations of leaf longevity in tropical moist forests predicted by a trait-driven carbon optimality model. *Ecology letters*, *20*(9), 1097–1106.

Xu, L., Samanta, A., Costa, M. H., Ganguly, S., Nemani, R. R., & Myneni, R. B. (2011). Widespread decline in greenness of Amazonian vegetation due to the 2010 drought. *Geophysical Research Letters*, *38*, L07402. https://doi.org/10.1029/2011GL046824

Yin, X., Struik, P. C., Romero, P., Harbinson, J., Evers, J. B., Van Der Putten, P. E., & Vos, J. A. N. (2009). Using combined measurements of gas exchange and chlorophyll fluorescence to estimate parameters of a biochemical C3 photosynthesis model: a critical appraisal and a new integrated approach applied to leaves in a wheat (Triticum aestivum) canopy. *Plant, cell & environment*, *32*(5), 448–464.